Elsevier Editorial System(tm) for Journal of Alloys and Compounds

Manuscript Draft

Manuscript Number: JALCOM-D-20-11372R1

Title: High temperature cyclic oxidation behavior of a low manganese Fe12Mn9Cr5Si4Ni-NbC shape memory stainless steels

Article Type: Full Length Article

Keywords: High temperature oxidation; Fe-Mn-Si-Cr-Ni; internal oxidation; manganese effect; silica

Corresponding Author: Dr. Artur Mariano de Sousa Malafaia, D.Sc.

Corresponding Author's Institution: Universidade Federal de São João Del Rei

First Author: Artur Mariano de Sousa Malafaia, D.Sc.

Order of Authors: Artur Mariano de Sousa Malafaia, D.Sc.; Rodrigo Silva, D.Sc.; Carlos A Della Rovere, D.Sc.; Renato Baldan, D.Sc.; Lucía Suárez-Fernández, D.Sc.; José M Cabrera-Marrero, D.Sc.; Marcelo F de Oliveira, D.Sc.

Abstract: High amounts of Mn in Fe-Mn-Si-Cr-Ni shape memory stainless steels are detrimental for oxidation resistance at high temperatures. However, in order to maintain the shape memory effect of these alloys the content of manganese must be between 12 and 17 wt.%. Thus, this study evaluated an alloy with relative low Mn (12 wt.%) in cyclic oxidation tests at 800, 900 and 1000 °C. Kinetic analysis demonstrated parabolic oxidation behavior with rate similar to higher Mn-containing alloys from literature. It was also observed internal oxidation, for the first time in these alloys, and oxide layers composed by Mn_2O_3 and Mn-Cr spinel at 800 °C as well as Mn-Cr spinel and no continuous silica at 1000 °C. The internal oxidation mechanism was related to oxide layer defects and not to partial oxygen pressure decrease, considering that the internal oxidation presented the same oxides of the external layer. These results show that low Mn content does not improve the use viability of these alloys at high temperatures, since no decreasing in oxidation rate was observed and further internal oxidation occurred.

Research Data Related to this Submission

There are no linked research data sets for this submission. The following reason is given:
Data will be made available on request

Cover Letter

Dear Editor,

Please find attached the revised manuscript entitled: **High temperature cyclic oxidation behavior of a low manganese Fe12Mn9Cr5Si4Ni-NbC shape memory stainless steels**, which we are submitting for publication in the *Journal of Alloys and Compounds*. The manuscript was restructured as requested by the reviewer. The main reasons why we believe it deserves to be published are based on the following justifications, as mentioned in the first submission:

i) A shape memory stainless steel FeMnSiCrNi with relative low manganese content (12 wt.%) was studied aiming to improve the limited oxidation resistance of Fe-Mn-Si-Cr-Ni alloys at high temperature. Cyclic oxidation tests were performed at 800, 900 and 1000 °C. However, the oxidation kinetics demonstrated that the mass gain rate of this alloy was similar of alloys with higher content of manganese, presenting parabolic mass gain rate.

ii) The low content of manganese was also related to an internal oxidation, phenomenon that has not been observed previously for this kind of alloy, independently of the manganese content, and the mechanism was explained.

iii) Finally, FEG-SEM/EDS, XRD were used to characterize the oxide layers formed and to compare with thermodynamic simulations prediction. Typical layer with Mn_2O_3 and $MnCr_2O_4$ oxides was observed at 800 °C and after tests at 1000 °C the oxides reported were Mn-Cr spinel and SiO_2 (the latter reported for the first time in these alloys above 700 °C).

Sincerely,

D.Sc. Artur Mariano de Sousa Malafaia

Prime Novelty Statement

The prime novelty of this paper is evaluating a low manganese Fe12Mn9Cr5Si4Ni-NbC shape memory stainless steels in cyclic oxidation at 800, 900 and 1000 °C. The relative low manganese (considering the composition of iron-based shape memory effect alloys) was proposed based on the detrimental effect of this element on oxidation resistance. However, the results demonstrated no decrease in mass gain rate. Furthermore, internal oxidation was reported for the first time in these alloys as also silica formation in temperatures above 700 °C. Finally, oxide layer characterization after oxidation at 1000 °C was never published before in this kind of alloy.

Response to Reviewers

Dear Editor Professor Livio Battezzati and Reviewer,

I would like to acknowledge the opportunity of reviewing the manuscript and all the comments. They helped improving the paper and below we reply the comments in bold.

Sincerely,

DSc. Artur Mariano de Sousa Malafaia

Reviewers' comments:

Reviewer #1: In this manuscript, the authors try to evaluate cyclic oxidation behavior of low Mn shape memory stainless steel and readers clearly understand the obtained results. However, reviewer think that quality of the manuscript doesn't reach the level of publication. The authors should think about the following points and revise the manuscript.

Thank you about your revision. All the points were taken into account in the revised manuscript.

1. Structure of the manuscript is not suitable for publication. The authors should divide "Results and Discussion" into 2 sections of "Results" and "Discussion". The authors should elucidate clearly the effect of Mn content (effect of decreasing Mn content) on oxidation behavior.

The paper was restructured and the Section "Results and Discussion" was separated. On the Discussion Section, the last subsection was dedicated to the internal oxidation, that was the main effect of using the lower manganese content.

2. Although the authors show phase stability diagram by Themo-Calc, most of readers are not familiar with this kind of diagram. Reviewer recommends that the authors elucidate chemical stability of the oxides just after showing all information about the oxide scale (XRD, Cross-section and EDS). It is much better for readers to show firstly the experimental results.

Thanks, the Thermo-Calc diagrams were presented only after XRD/SEM/EDS characterization of each temperature.

3. If the authors show XRD patterns, the authors also mention the penetration depth of incident X-ray.

This information is difficulted as different oxides were formed and the penetration depth is dependent of density, flat interfaces, homogeneity and cracks or porosity also modify this value. However, some commentaries were added to make clear that the XRD depth penetration was enough to pass the oxide scale and reach the ferritic Mn-depleted substrate.

Highlights

Parabolic mass gain rate with similar k_p of higher Mn-content alloys was observed

Internal oxidation was observed for the first time in these alloys

Typical Mn_2O_3, $MnCr_2O_4$ oxide layer at 800 °C was characterized by XRD and SEM/EDS

SiO_2 non-continuous layer was evidenced at metal/oxide interface after test at 1000 °C

Critical Mn-depletion and cyclical stresses were associated to internal oxidation

Figure 1

Click here to download high resolution image

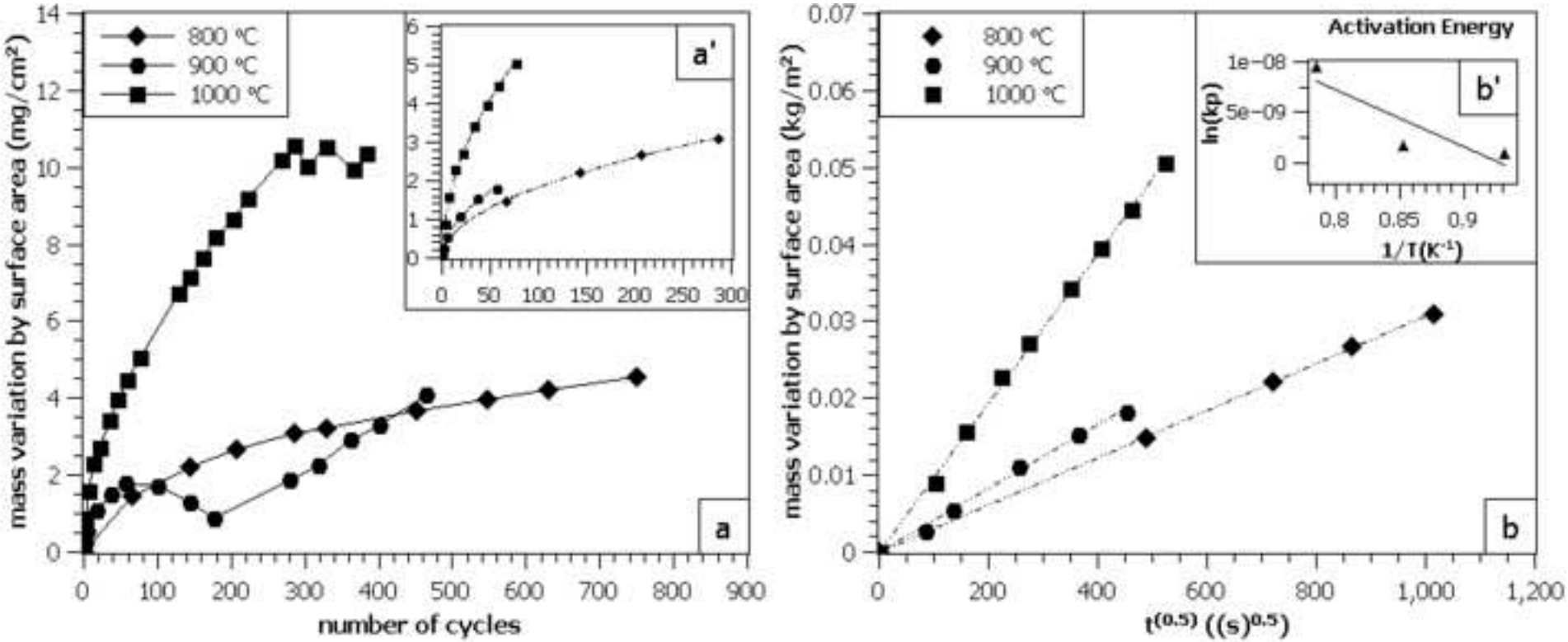

Figure 2

Click here to download high resolution image

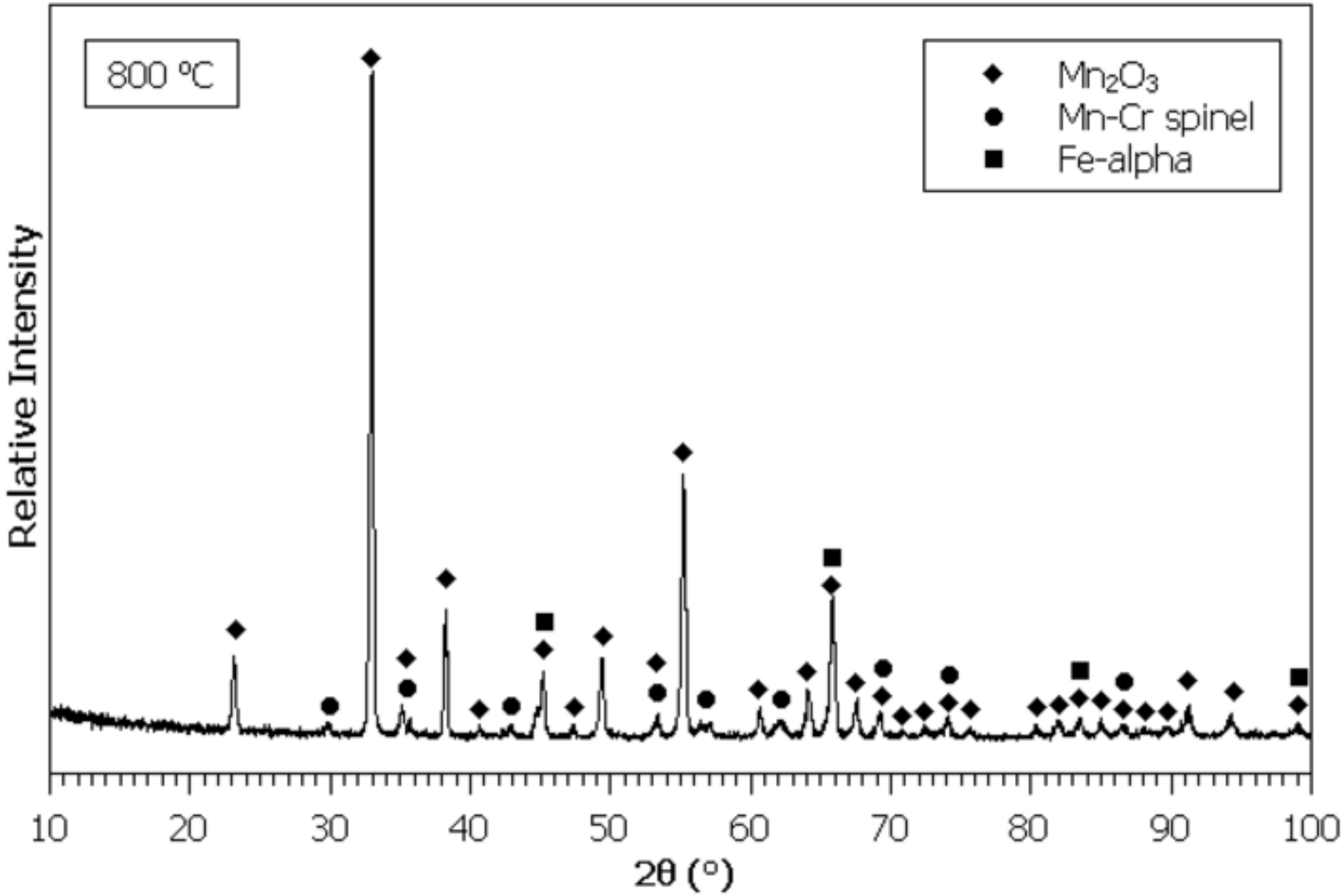

Figure 3

Click here to download high resolution image

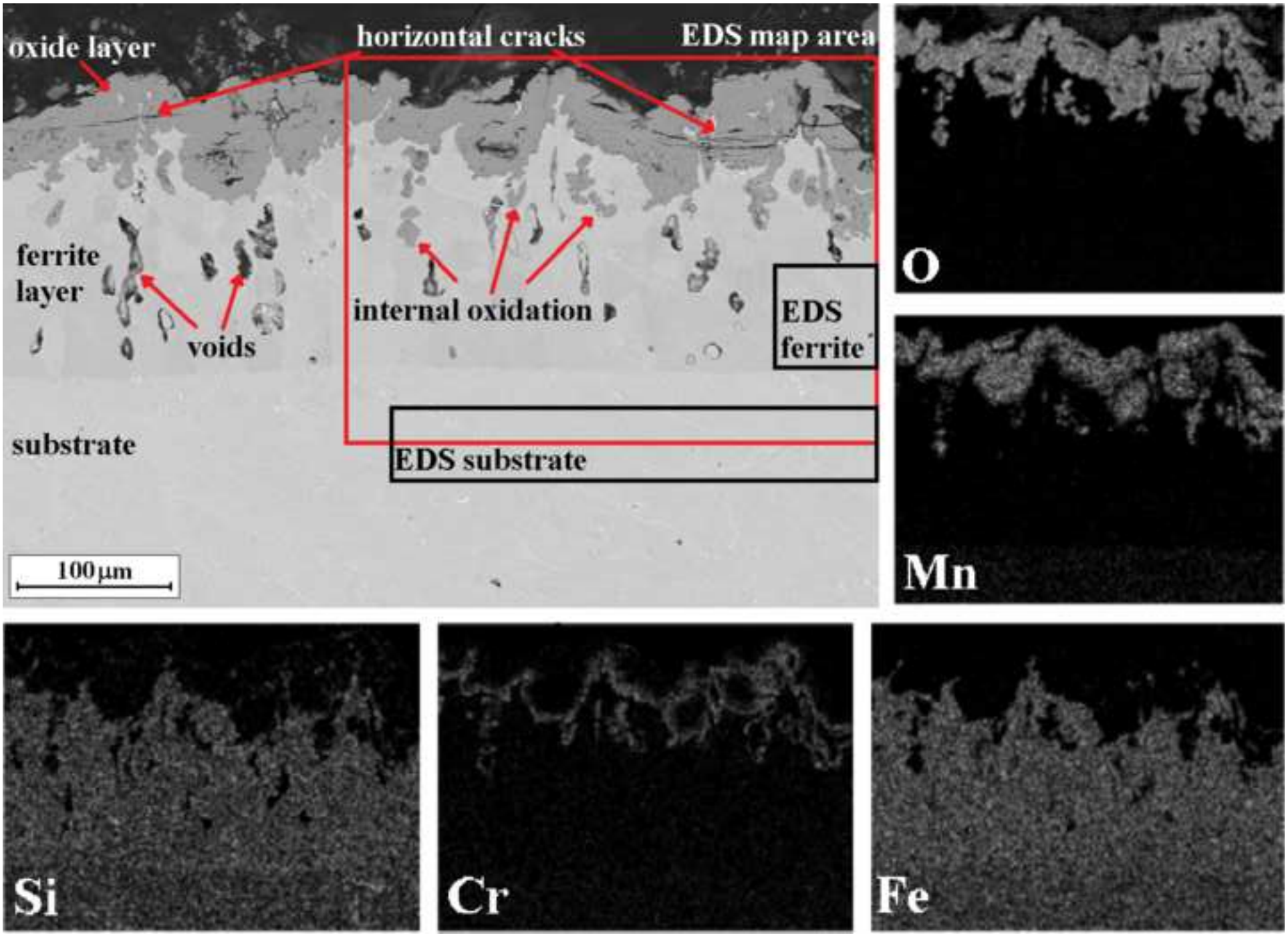

Figure 4

Click here to download high resolution image

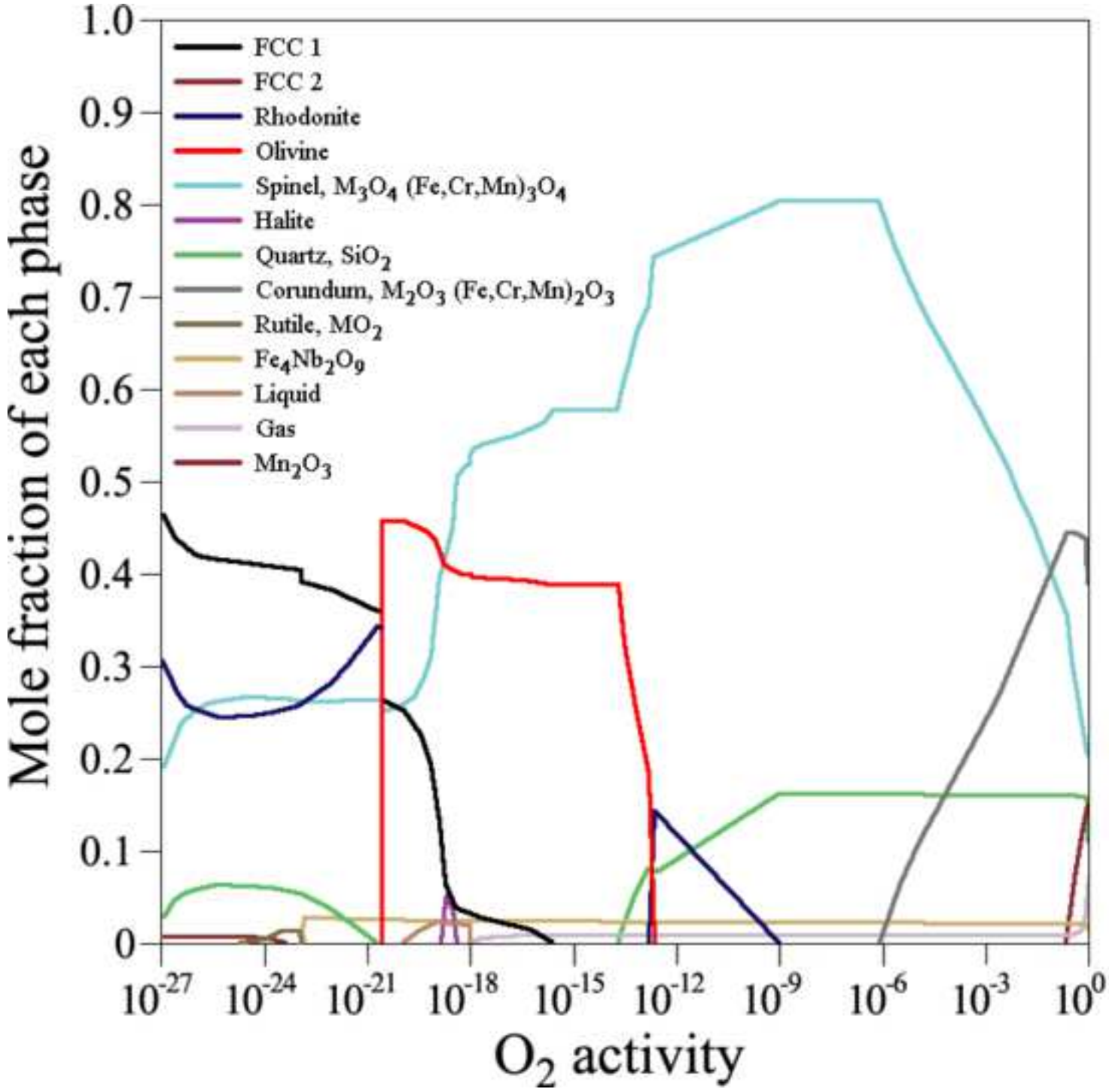

Figure 5

Click here to download high resolution image

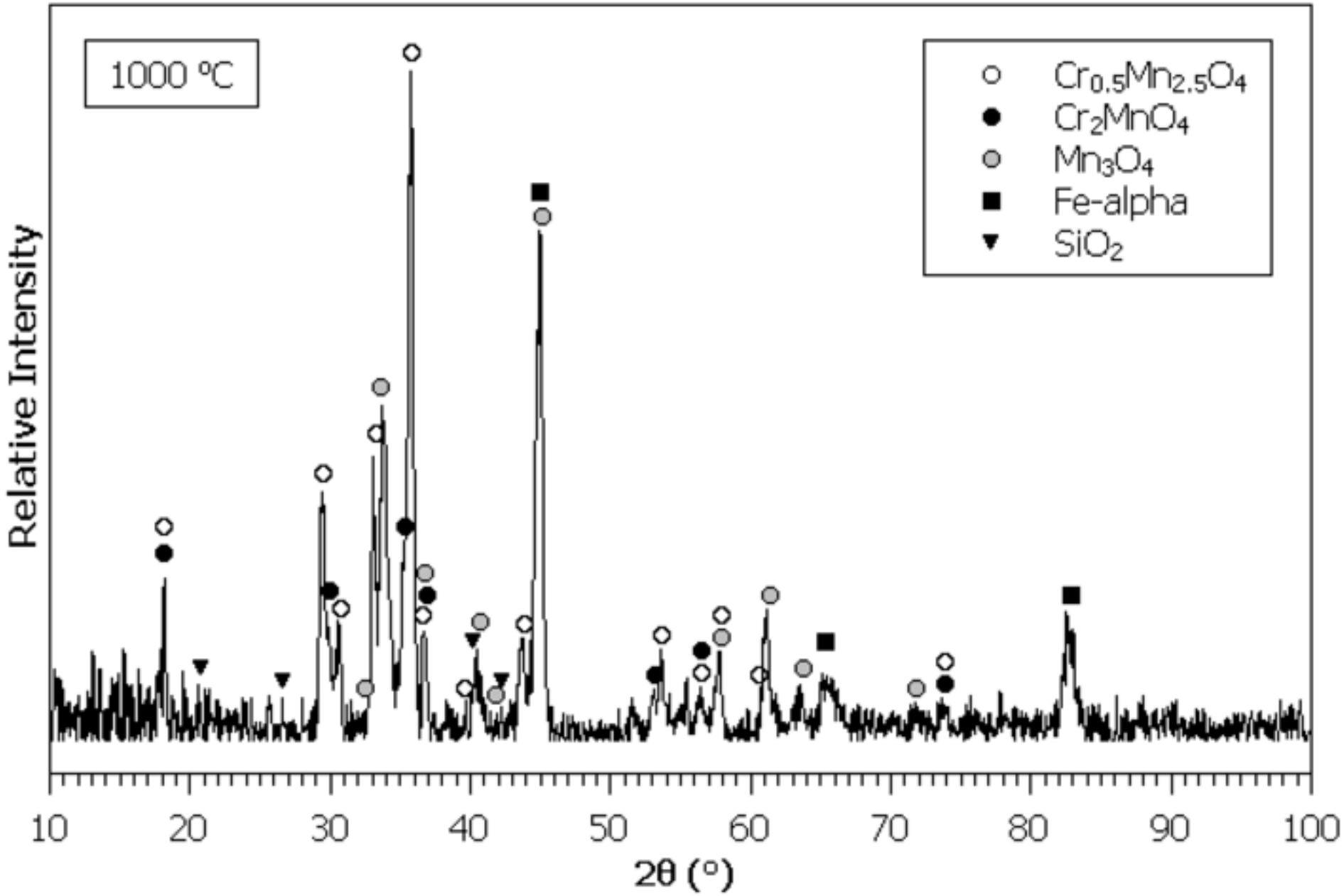

Figure 6

Click here to download high resolution image

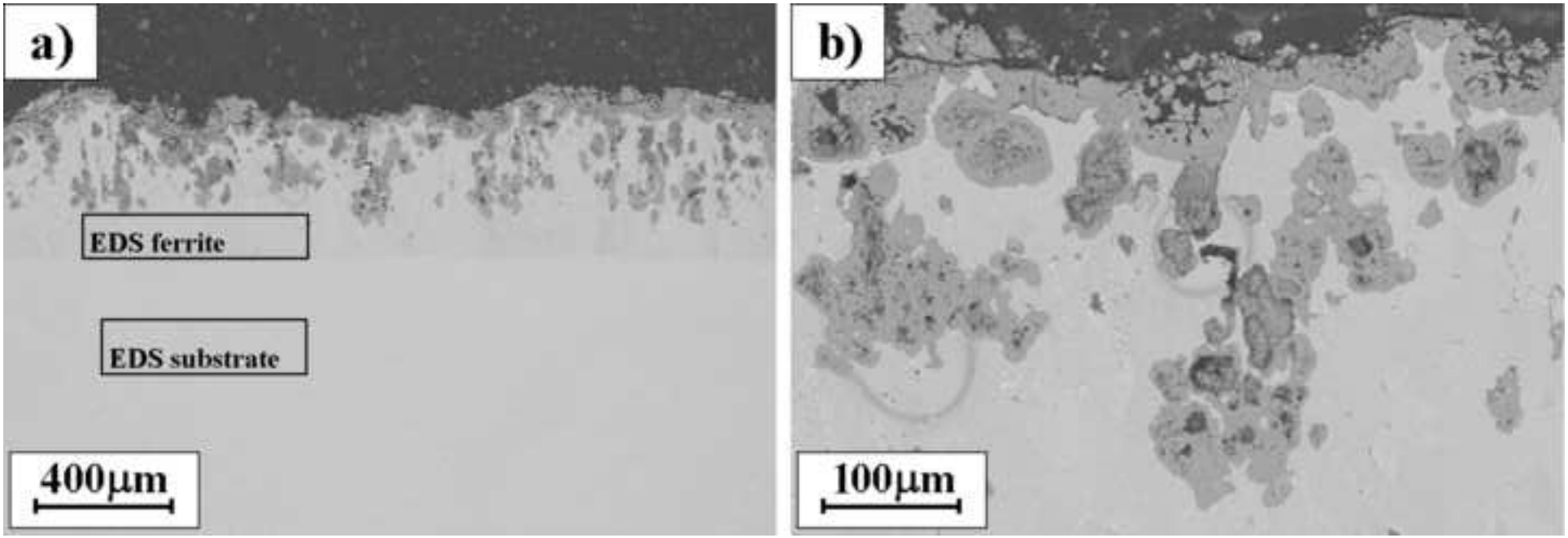

Figure 7

Click here to download high resolution image

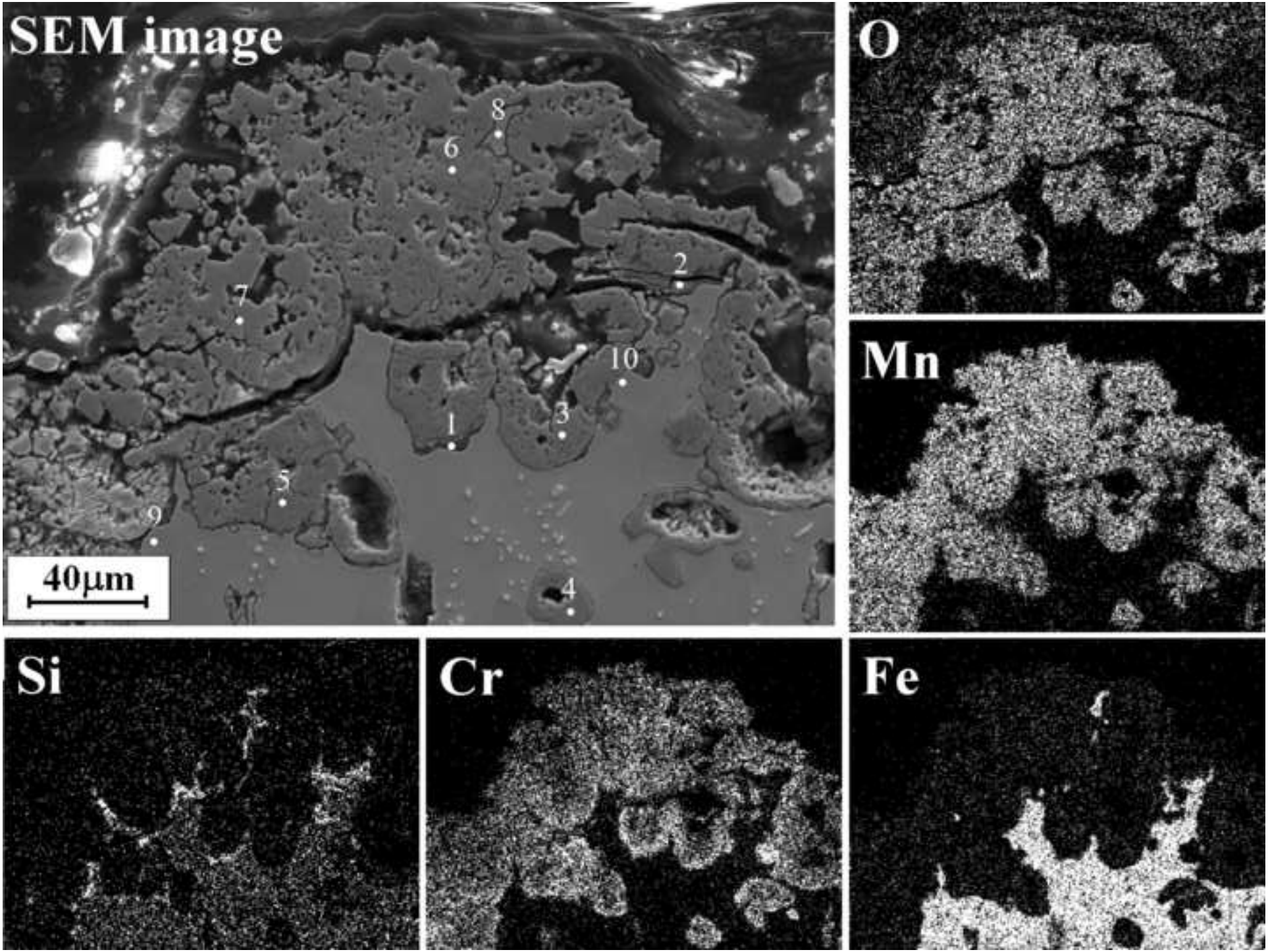

Figure 8
Click here to download high resolution image

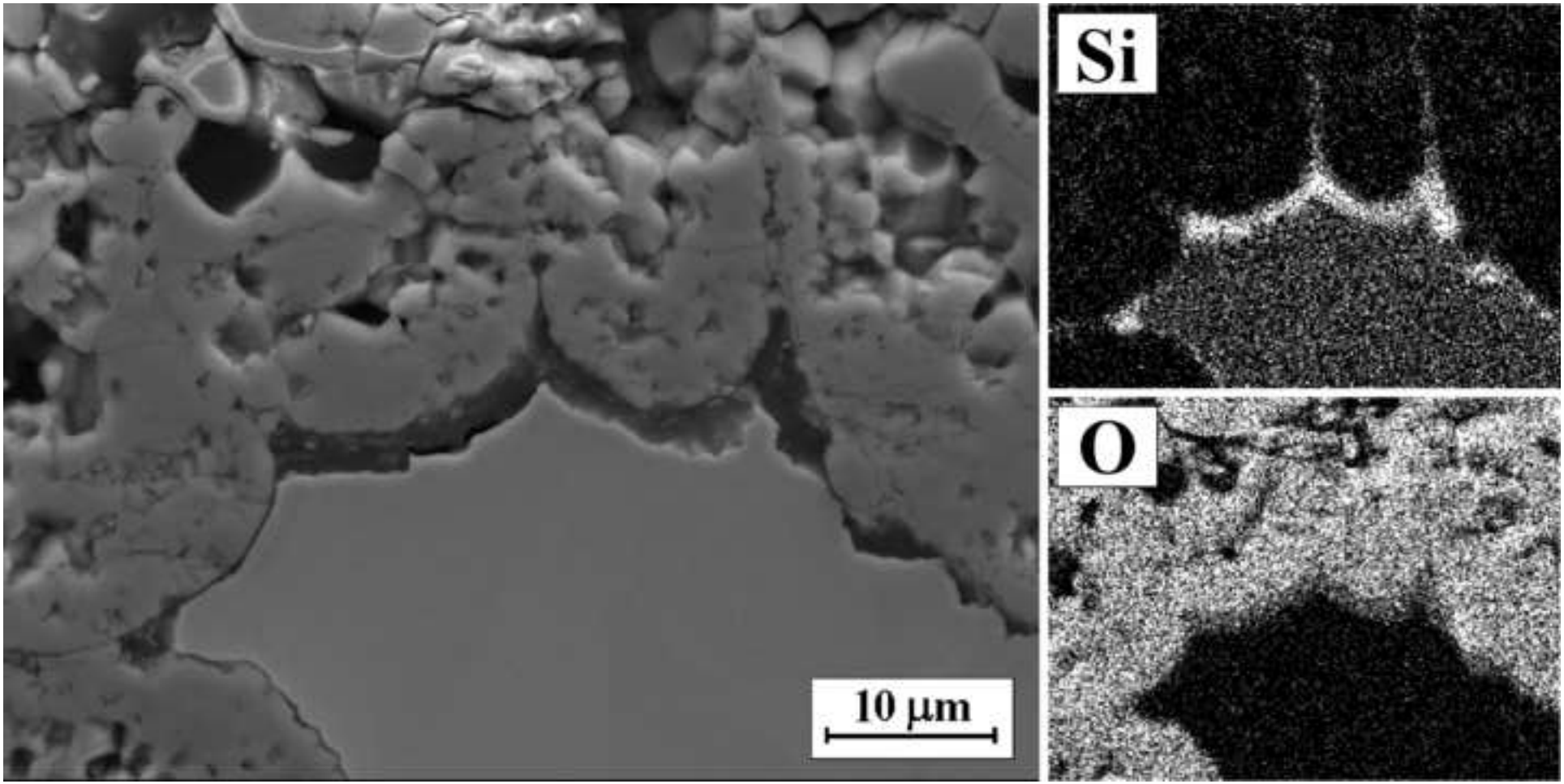

Figure 9

Click here to download high resolution image

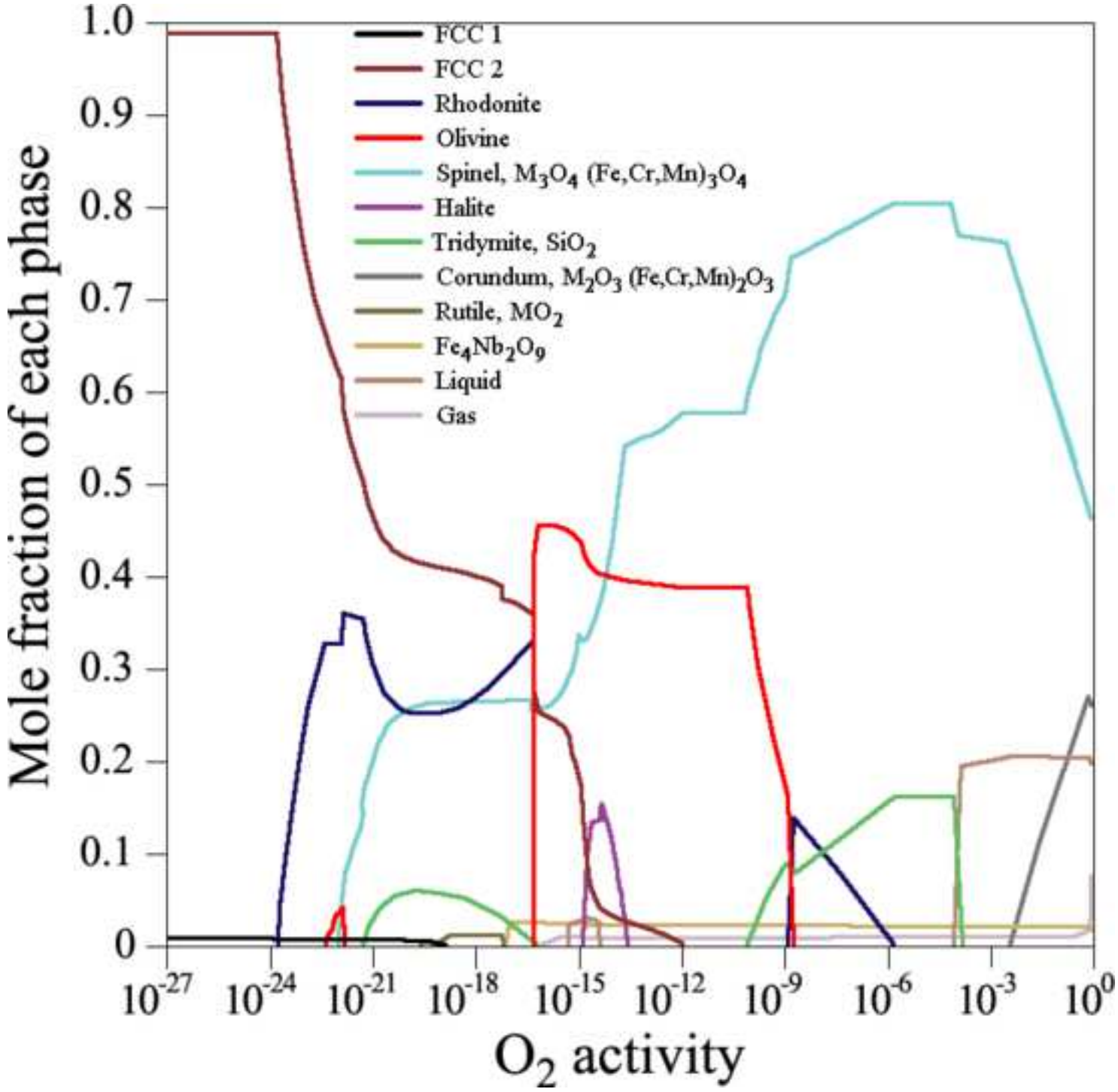

Figure 10

Click here to download high resolution image

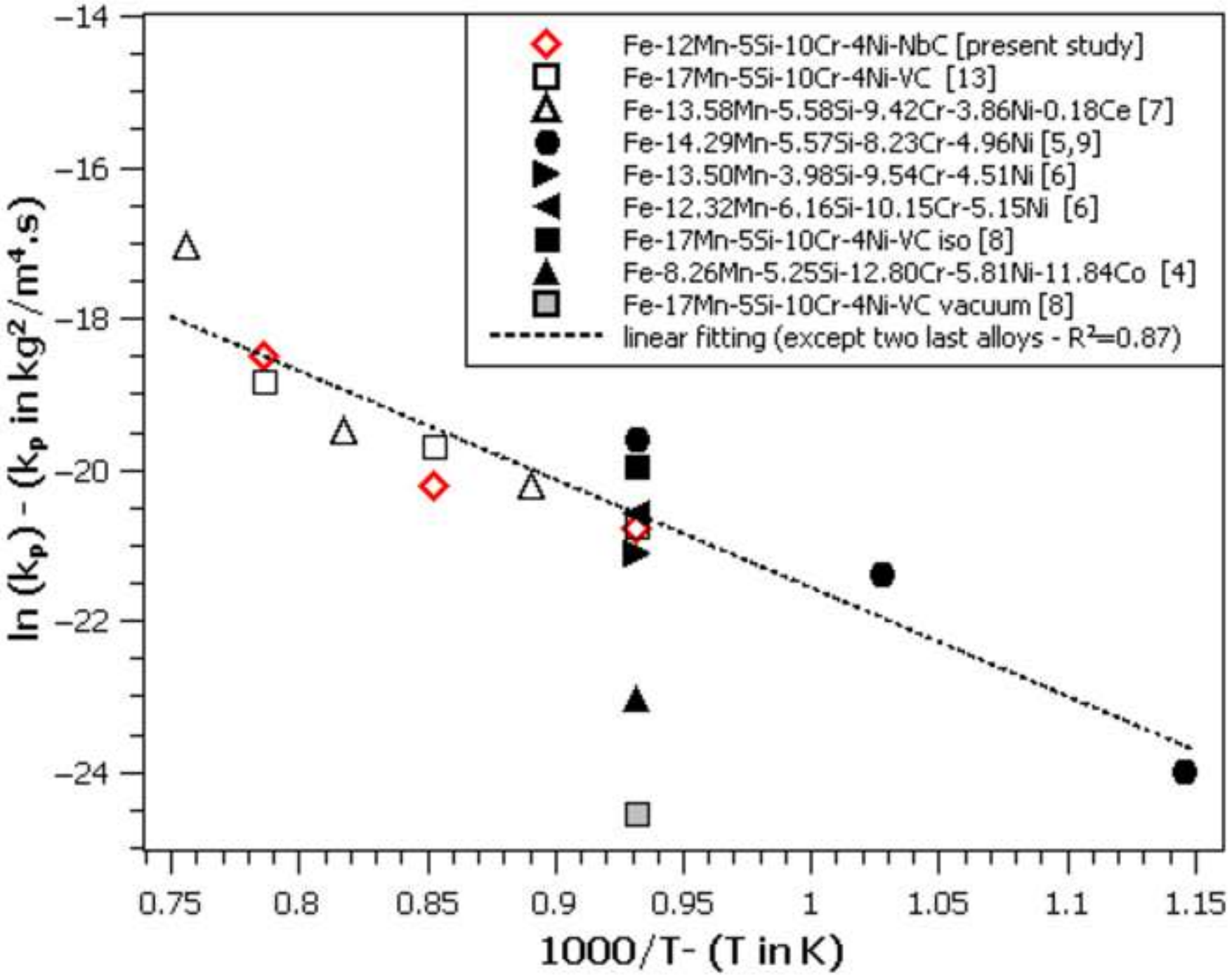

***Credit Author Statement**

CRediT author statement

Artur Mariano de Sousa Malafaia: Conceptualization, Methodology, Investigation, Writing- Original draft preparation, Writing- Reviewing and Editing **Rodrigo da Silva:** Visualization, Writing- Reviewing and Editing **Carlos Alberto Della Rovere:** Writing- Reviewing and Editing **Renato Baldan:** Writing- Reviewing and Editing **Lucía Suárez-Fernández:** Supervision, Writing- Reviewing and Editing **José-María Cabrera-Marrero:** Resources, Writing- Reviewing and Editing **Marcelo Falcão de Oliveira:** Conceptualization, Methodology, Resources, Supervision, Writing- Reviewing and Editing.

***Declaration of Interest Statement**

Declaration of interests

☒ The authors declare that they have no known competing financial interests or personal relationships that could have appeared to influence the work reported in this paper.

☒The authors declare the following financial interests/personal relationships which may be considered as potential competing interests:

None

High temperature cyclic oxidation behavior of a low manganese Fe12Mn9Cr5Si4Ni-NbC shape memory stainless steels

Artur Mariano de Sousa Malafaia[a,*], Rodrigo da Silva[b], Carlos Alberto Della Rovere[b], Renato Baldan[c], Lucía Suárez-Fernández[d], José-María Cabrera-Marrero[e,f], Marcelo Falcão de Oliveira[g]

a São João Del Rei Federal University (UFSJ), Campus Santo Antônio, Praça Frei Orlando, 170, Centro, 36307-352, São João Del Rei/MG, Brazil, +55 32 33795879, +55 32 999007605

* Corresponding author: arturmalafaia@ufsj.edu.br

b Munir Rachid Corrosion Laboratory, Department of Materials Engineering, Federal University of São Carlos, Rodovia Washington Luis Km 235, 13565-905 São Carlos, SP, Brazil

c São Paulo StateUniversity (Unesp), Campus of Itapeva, Rua Geraldo Alckmin 519, Vila Nossa Senhora de Fátima, 18409-010, Itapeva/SP, Brazil.

d Idonial Centro Tecnológico, Parque Empresarial Principado de Asturias C) Calafates. Parcela L-3.4, 33417 Avilés, Asturias, Spain

e Department of Materials Science and Engineering, Polytechnic University of Catalunya, EEEB, c/Eduard Maristany 10-14, 08019 Barcelona, Spain (permanent address)

f Institute for Research in Metallurgy and Materials, Universidad Michoacana de San Nicolás de Hidalgo, Edificio “U-3”, Ciudad Universitaria, 58030, Morelia, Michoacán, Mexico (present address)

gSão PauloUniversity, Av. João Dagnone, 1100, Jd. Sta. Angelina, São Carlos-SP, 13563-120, Brazil.

Abstract

High amounts of Mn in Fe-Mn-Si-Cr-Ni shape memory stainless steels are detrimental for oxidation resistance at high temperatures. However, in order to maintain the shape memory effect of these alloys the content of manganese must be between 12 and 19 wt.%. Thus, this study evaluated an alloy with relative low Mn (12 wt.%) in cyclic oxidation tests at 800, 900 and 1000 °C. Kinetic analysis demonstrated parabolic oxidation behavior with rate similar to higher Mn-containing alloys from literature. It was also observed internal oxidation, for the first time in these alloys, and oxide layers composed by Mn_2O_3 and Mn-Cr spinel at 800 °C as well as Mn-Cr spinel and no continuous silica at 1000 °C. The internal oxidation mechanism was related to oxide layer defects and not to partial oxygen pressure decrease, considering that the internal oxidation presented the same oxides of the external layer. These results show

that low Mn content does not improve the use viability of these alloys at high temperatures, since no decreasing in oxidation rate was observed and further internal oxidation occurred.

Keywords

High temperature oxidation; Fe-Mn-Si-Cr-Ni; internal oxidation; manganese effect; silica.

Introduction

The Fe-based shape memory alloys (SMA) Fe-Mn-Si-Cr-Ni were developed as a cheapest alternative option to traditional NiTi SMA [1,2]. Furthermore, studies demonstrated that this kind of alloy can be used to join tubes by the shape memory effect [3] and have suggested applying them at high temperature [4]. Despite the high percentage of Mn being a problem for metallic alloys employed at high temperatures, in the last decade, studies regarding high temperature oxidation of this austenitic alloys were developed. For instance, Ma et al. [5] reported, for an Fe-14.29Mn-5.57Si-8.23Cr-4.96Ni alloy, a mass gain more than ten times higher than the conventional stainless steel AISI 304 after 100 h at 800 °C. They observed that during oxidation at high temperature the oxide layer presents Mn-rich oxides (Mn_2O_3 and Mn_3O_4) and Mn-Cr-spinel, causing depletion of Mn and generating a ferrite layer near the metal/oxide interface. After that, several studies were developed in order to try improving the oxidation resistance of these alloys, named as shape memory stainless steels (SMSS) [4,6–8].

As this kind of alloy presents Si and Cr, that are known to provide high oxidation resistance in Fe-based alloys, an obvious attempt for improving the performance at high temperature would be to increase Cr and Si as well as to decrease Mn amount. Comparing two SMSSs, Fe-13.50Mn-3.98Si-9.54Cr-4.51Ni and Fe-12.32Mn-6.16Si-10.15Cr-5.15Ni [6], it was observed that the second one, with less Mn and larger amount of ferrite stabilizers elements, Si and Cr, presented superior mass gain under isothermal oxidation at 800 °C. The explanation was that higher amounts of Si and Cr, both ferrite-stabilizers elements, facilitated ferrite stabilization at 800 °C during oxidation due to Mn depletion, making the Mn diffusion rate faster when compared with the austenitic structure [9]. Additions of Co [4] have been also efficient to reduce at least half the mass gain in isothermal oxidation at 800 °C. However, the Fe-8.26Mn-5.25Si-12.80Cr-5.81Ni-11.84Co alloy is more expensive and present a generalized precipitation of intermetallic phases due to exposure to high temperature. Addition of Ce [7] was also used as a way to improve oxidation resistance during cyclic tests at 850, 950 and 1050 °C, in an Fe-13.58Mn-5.58Si-9.42Cr-3.86Ni-0.18Ce, but the mass gain was similar to that of conventional SMSSs. Indeed, the mechanism related to Ce alloying has not been deeply investigated yet.

One effective way proposed in the literature for an Fe-17Mn-5Si-10Cr-4Ni-VC alloy [8] to decrease mass gain is the application of a vacuum pre-treatment to promote Mn volatilization aiming to form a ferrite layer (~170 μm in thickness), depleted in Mn upon the austenite substrate. In this way, the oxidation rate at 800 °C, during 24 h exposure, was two

orders of magnitude smaller than that in samples without vacuum pre-treatment. Similarly, vacuum annealing also improved aqueous corrosion resistance of an Fe-17.5Mn alloy [10]. Mn depletion was also achieved by pre-oxidation and oxide removal. This strategy has been used in an Fe 28.0Mn-6.15Si-5.16Cr to improve both passivity and corrosion resistance [11], and in an Fe-18.81Mn-5.61Si-9.31Cr-5.36Ni [12] to create a smart material, with shape memory effect and magnetic properties, generated by the ferrite layer presence.

Oxidation resistance for other temperatures have also been evaluated for SMSSs. For instance, in an Fe-14.29Mn-5.57Si-8.23Cr-4.96Ni, a SiO_2 layer was easier formed at 600 °C than at 700 and 800 °C, but the oxide layer was again mainly formed by Mn-oxides after isothermal oxidation [9]. In cyclic oxidation, Fe-17Mn-5Si-10Cr-4Ni-0.59V-0.14C tested at 800, 900 and 1000 °C presented also high mass gain coefficients, and an activation energy of 109 kJ/mol related to oxide layer formation [13]. This value is considerably smaller than 247 kJ/mol, that was observed for conventional chromia-forming stainless steel [14], showing the lower oxidation resistance provided by the SMSSs. The oxide layers were characterized only after oxidation at 900 °C (identifying typical Mn and Cr presence) because this material presented an anomalous oxidation behavior at this temperature. After some oxide spallation and mass loss, the material returned to gain mass. This uncommon behavior was first related to the roughness increase at the metal/oxide interface, generated by ferrite layer plastic deformation [13,15]. After that, a comparison between isothermal and cyclic oxidation was performed at 950 °C for the Fe-13.58Mn-5.58Si-9.42Cr-3.86Ni-0.18Ce alloy [16], demonstrating that the roughness increasing at metal/oxide interface is derived from a chemical and mechanical combined effect, as the isothermally oxidized samples also presented rough interfaces in a low degree when compared to cyclic oxidized samples.

The present study was performed in an Fe-12Mn-5Si-9Cr-4Ni-1Nb-0.1C alloy under cyclic oxidation at 800, 900 and 1000 °C. Niobium and carbon were used to improve the mechanical resistance at high temperatures, as reported for other steels [17,18], and also considering that niobium carbides were already used to improve the shape memory effect in Fe-Mn-Si-Cr-Ni alloy [19]. The main aim here was to identify if an alloy with less amount of Mn (compared to the literature) could present a better oxidation resistance by evaluating its oxidation kinetics. Furthermore, to check if the anomalous behavior during cyclic oxidation also occurs for this alloy and to characterize the oxides formed by means of scanning electron microscopy with a field emission gun in conjunction with energy-dispersive X-ray spectroscopy (FEG-SEM/EDS) and X-ray diffraction (XRD) analyses.

Materials and Methods

The Fe-12Mn-5Si-9Cr-4Ni-1Nb-0.1C alloy (nominal composition in mass percentage) was melted in an induction furnace and sand casted. After cast, the alloy was homogenized at 800 °C for 3 h. The chemical composition was verified by EDS and carbon was determined by combustion. For the oxidation tests, samples were extracted from the ingot and grounding until #600 SiC sandpaper. The samples dimensions for higher temperatures were approximately 15×10×4 mm, while for 800 °C the size was 25×25×12,5 mm. The sample dimensions were larger at the lowest temperature to evaluate wear resistance after oxidation, not presented here, as already performed for other alloys in a previous study [20]. Regarding the smaller samples size, they followed literature recommendations [21].

The cyclic oxidation tests were performed in air lab, using cycles with 1h hour at maximum temperature (800, 900 or 1000 °C) and 10 minutes of cooling in an automatic furnace. The mass change was measured in arbitrary interval of cycles and the tests were performed during 749 cycles at 800 °C, 465 cycles at 900 °C and 383 cycles at 1000 °C. The tests durations were related to material performance and, thus, were obviously shorter for higher temperatures. Thermodynamic simulations were performed using Thermo-Calc software (TCFE7 database) to predict the oxides expected at 800 and 1000 °C according to oxygen partial pressure ($p(O_2)$). Finally, aiming to understand the oxidation behaviour, the oxidised samples tested at 800 and 1000 °C were characterized by XRD, using Cu-K_α radiation on top surface, and by FEG/SEM and EDS analyses on the cross-sections.

Results

Chemical analysis, Mass variation and Oxidation kinetics

Regarding the alloy chemical composition, the EDS analysis determined the following: Fe-12.0Mn-5.3Si-8.8Cr-3.9Ni-1.5Nb-0.07C. The oxidation tests were then carried out and the Figure 1a shows the mass variation observed in the three temperatures by the number of cycles while Figure 1b presents the parabolic law fittings using mass gain by time square root, allowing the kinetics calculations. The alloy did not present mass loss at 800 °C, but presented mass loss at 900 °C, followed by a new mass gain. Before this behavior, the mass variation curve of the sample tested at 900 °C followed a parabolic law during some number of cycles, as occurred for other temperatures, as shown in detail in Figure 1a'. At 1000 °C, mass gain was observed during almost all the test, followed by some oscillation (loss and mass gain) at the end. Figure 1b' presents the plot of neperian logarithms of k_p values by the inverse of temperature in Kelvin used to calculate the activation energy (Arrhenius plot). Table 1

summarizes the values determined and one can see that the fittings to the parabolic law are in good agreement (Figure 1a' and b), with R^2>0.99 in all the cases. On the other hand, the linear fitting implemented to determine the activation energy presented R^2=0.89, although it is clear that some of the points are certainly far from the trending line.

Table 1 – Summarized data of parabolic coefficients (k_ps) determined for all the temperatures, the activation energy (E_a) and the pre-exponential factor (k_0) obtained from the Arrhenius plot.

Temperature (°C)	Number of total cycles	k_p ($kg^2/m^4.s$)	Interval cycles (following k_p)	R^2
800	749	$9.43x10^{-10}$	0-286	0.999
900	465	$1.67x10^{-9}$	0-57	0.995
1000	383	$9.46x10^{-9}$	0-76	0.998
E_a = 128.7 kJ/mol	(R^2=0.893)	$k_0 = 1.42x10^{-3}$ $kg^2/m^4.s$		

Oxide and Sub-scale Characterization

Oxidation at 800 °C

In the present study, the characterization was focused on the samples oxidized at 800 and 1000 °C, as the anomalous behavior observed for the oxidized sample at 900 °C was previously reported regarding a similar alloy under the same oxidation conditions [13]. Figure 2 presents the XRD measurements performed on the sample surface after oxidation at 800 °C (749 cycles). Regarding the oxide formation, the main contribution observed was Mn_2O_3 followed by a spinel Mn-Cr, and also Fe-α peaks.

Figure 3 presents the cross-section of the sample oxidized at 800 °C, after 749 cycles, and observed by SEM/EDS. Several important characteristics can be pointed out by SEM image. First, the oxide layer presents some horizontal cracks. Second, the metal/oxide interface developed a substantial roughness. Third, a characteristic metallic layer was formed between the oxide layer and the metal substrate, with a quite flat interface between them. EDS analyses in this region demonstrated a Mn content of 1.2 wt.%, while in the substrate, near the ferrite/austenite interface, 12.8 wt.% was observed. A Cr depletion is also noted, containing 8.8 wt.% in the substrate whereas 6.2 wt.% in the Mn-depleted zone. Fourth, some defects and a lot of globular oxide particles were also observed in this layer. In the cross-sectional EDS maps, it can be noticed that the oxide layer is mainly formed by Mn and present Cr near the metal/oxide interface. In the oxidized particles surrounded by metal, a similar behavior occurs with Mn enrichment in the center and Cr near the oxide/metal interface. The already mentioned Mn-depleted metallic layer, between the oxide and the substrate, could be observed, in which Cr depletion was also noticed.

Thermo-Calc simulation for the expected phases at 800 °C as function of the $p(O_2)$ is presented at Figure 4. Although these simulations do not consider composition changes, as manganese and chromium depletion observed at SEM/EDS analysis (Figure 3), as also does not consider the formation rates of different oxides, it is still interesting to compare these predictions with oxide characterization. The simulation shows the predominance of corundum (M_2O_3) and spinel (M_3O_4) phases for high values of $p(O_2)$, followed by quartz (SiO_2). Due to the Nb content in the alloy, the presence of an $Fe_4Nb_2O_9$oxide is also calculated, but it is expected in a low amount. As the $p(O_2)$ decreases the spinel amount expected increases and the presence of other oxide structures are suggested (not detailed here as they were not observed by oxide characterization).

Oxidation at 1000 °C

Figure 5 shows the XRD results for the sample oxidized at 1000 °C during 383 cycles. M_3O_4 spinel oxides are noticed in higher amount, with larger concentration of Mn (Mn_3O_4 and $Cr_{0.5}Mn_{2.5}O_4$-tetragonal) or Cr (Cr_2MnO_4-cubic). Furthermore, some silica peaks could be identified, with some doubt due to the background and/or superposition of other oxide peaks. Finally, Fe-α peaks related to the ferrite layer formation were also observed.

Figure 6 presents the cross-section image of a sample oxidized at 1000 °C during 383 cycles. Similar characteristics to the sample oxidized at 800 °C can be observed: internal oxidation, Mn-depleted zone, roughness at the metal/oxide interface and the ferrite layer, with a quite flat interface with austenite (Figure 6a). The internal oxidation was more intense at this temperature (Figure 6b). While at 800 °C the more internal globular oxide particles were placed around 100 μm far from the metal/oxide interface, at 1000 °C this value is higher than 200 μm. However, in both cases the internal oxidation was confined to the ferrite layer. In addition, EDS analysis revealed that Mn-depleted zone also suffered a higher Cr depletion. The Mn decreases from 12.0 to 0.9 wt.%, while Cr from 8.8 to 2.7 wt.%.

Figure 7 brings a more detailed EDS analysis with some maps and spots (compositions presented in Table 2). Nb, C and Ni maps were not added as they appeared only in the metallic phases. The EDS maps and micro-analyses in the points 1 and 2, performed at the metal/oxide interface, demonstrates the higher presence of Si in the oxide layer and the Figure 8 details a region where a non-continuous silicon-rich oxide was formed at metal/oxide interface, with approximately 2 μm in thickness. The EDS micro-analyses related to the points 3 through 7 (in Figure 7) demonstrated, as indicated by Cr and Mn maps (see also Figure 7) that the oxide layer is mainly composed by a Cr-Mn mixed oxide. Finally, the EDS measurements at points 8, 9

and 10 were done in metallic regions near the metal-oxide interface (point 8 is in a small "island" of metal inside the oxide layer). The depletion of Mn and Cr can be noticed in these regions, where 1.0≤Mn wt.%≤1.5 and 2.4≤Cr wt.%≤3.3, far from the original composition.

Table 2 – EDS chemical micro-analysis in wt.% (points in the Figure 7).

EDS point	Chemical elements						
	O	Si	Cr	Mn	Fe	Ni	Nb
1	41.3	22.0	7.2	3.4	23.0	1.7	1.3
2	47.4	17.2	9.0	16.5	7.7	0.9	1.4
3	33.8	---	21.5	42.6	2.2	---	---
4	35.0	---	34.8	26.8	3.5	---	---
5	34.8	---	33.0	29.8	2.4	---	---
6	37.2	2.7	27.3	30.9	1.9	---	---
7	29.5	---	23.2	45.4	2.0	---	---
8	---	4.4	3.3	1.5	86.5	4.3	---
9	---	5.8	2.4	1.0	86.0	4.8	---
10	1.9	5.9	2.9	1.2	83.2	5.0	---

Phases and its amounts were also predicted by thermodynamic simulation using Thermo-Calc for different $p(O_2)$ at 1000 °C, as shown in Figure 9. The oxide expected in larger amount at high $p(O_2)$ values is the spinel M_3O_4. Corundum oxide (M_2O_3) also appears, but in less percentage compared to 800 °C and limited for $p(O_2)$ values higher than 10^{-3}. A not expected phase is the liquid, as no melting was observed during oxidation tests. The Fe-Nb oxide appears again in small amount and SiO_2 (tridymite at this temperature) is expected only after $p(O_2)$ is reduced below approximately 10^{-4}.

Discussion

Chemical analysis, Mass variation and Oxidation kinetics

Although EDS is not the best technique to chemical analysis, the evaluation demonstrated a good accordance with the nominal composition, with relatively higher niobium and slight low chromium and carbon. However, the correct manganese content (12.0 wt%) was the result most important for the study purpose.

Regarding the mass variation (Figure 1), the behavior observed at 900 °C was reported previously for an Fe-17Mn-5Si-10Cr-4Ni-VC and considered anomalous [13,15] as usually, after the spallation start, the alloy presents continuous mass loss under cyclic oxidation. At 800 °C, it is important noticing that no spallation was observed during oxidation what is a detrimental

behavior of some austenitic stainless steels at high temperature [14]. The kinetics analysis demonstrated that for all temperatures a good agreement to the parabolic law was observed (Figure 1b and Table 1). Comparing the present results with a higher Mn content Fe-17Mn-Si-Cr-Ni-0.59V-0.14C alloy (nominal composition in wt.%) previously studied [13], and tested under the same conditions, the reduction of Mn was not enough to reduce the mass gain during oxidation; at 800 °C the k_p value is similar, being considerably lower at 900 °C and higher at 1000 °C. This comparison can help to understand the deviation observed here in the Arrhenius plot (Figure 1b'), which can be attributed for the spallation behavior observed at 900 °C. As the spalled oxide was not collected, it can have been started since the first cycles, generating a smaller k_p value that is far from the trending line and not allowing a better fitting.

Correlating k_p values between isothermal and cyclic tests is sometimes avoided as in cyclic tests the samples are more prone to suffer oxide spallation, as mentioned before. However, in Figure 10, literature values of k_p are put together for comparative purposes in an Arrhenius plot, where open symbols accounts for cyclic tests and filled symbols for isothermal ones. A hypothetical linear fitting is presented (R^2=0.87), excluding the points regarding the alloy with Co [4] and the alloy oxidized after vacuum annealing [8], showing that for all the other alloys, independently of the Mn content there is a similar and high mass gain. Clearly, the only successful attempts for decreasing mass gain during oxidation in air at high temperature in these SMSS alloys were, therefore, through the Co addition or vacuum annealing. Thus, the use of a reduced Mn-content alloy here was not able to generate a better oxidation resistance in SMSSs.

Oxide and Sub-scale Characterization

Oxidation at 800 °C

The results observed by XRD after oxidation at 800 °C (Figure 2) and SEM/EDS (Figure 3) are in agreement with oxides observed and analyzed by XRD and EDS on Fe-Mn-Si-Cr-Ni alloys in previous studies [4-6]. These authors found Mn_2O_3, in the external layer basically, Mn_3O_4 at middle layer and $MnCr_2O_4$ located at the metal/oxide interface. Furthermore, it was reported that a Mn-depleted zone was formed below the oxide layer [4-7,11,13], where a metallic transformation from austenite to ferrite occurs. This fact explains the Fe-α peaks observed by XRD. Although the oxide layer formed was thick, reaching more than 50 μm in some regions (Figure 3) the defects and regions with lower thickness allowed substrate peaks determination. Here, the main Mn_2O_3 contribution and small peaks of $MnCr_2O_4$ are in accordance with oxides distribution and the high Mn_2O_3 thickness (Figure 3). The Mn_3O_4 oxide

was not observed here, but in one of the previous studies it was necessary to remove partially the oxide layer to characterize this oxide by XRD [5].

The XRD results for the sample oxidized at 800 °C are also in agreement with the phase diagrams obtained from thermodynamic simulations of Cr-Mn-O system [22,23], where the stable oxide, regarding the present Cr/(Mn+Cr) ratio (around 0.45), is only cubic spinel ($Mn_xCr_{3-x}O_4$, where $0 \leq x \leq 3$). However, the fast manganese diffusion probably decreases the Cr/(Mn+Cr) ratio to values below 0.4 where Mn_2O_3 is also stable. On the other hand, as Mn is depleted (increase of Cr/(Mn+Cr) ratio) and the $p(O_2)$ is decreased, the equilibrium is moved towards the stabilization of the cubic spinel alone [22,23]. Furthermore, the oxides predicted by Thermo-Calc here, as also already reported for three Fe-Mn-Si-Cr-Ni alloys [5,6] are in accordance with the increase of $MnCr_2O_4$ phase as $p(O_2)$ decreases (Figure 4). Regarding the other phases predicted by Thermo-Calc simulation (Olivine, Rhodonite, Halite and so on) none of them were found here or reported during previous characterization of Fe-Mn-Si-Cr-Ni alloys oxidized [4–8,13]. Silica oxide was also never observed in these alloys after oxidation at 800 °C, although it was reported after oxidation at 600 °C [9]. With respect to Mn-rich oxides, in pure manganese, Mn_2O_3, Mn_3O_4 and MnO are expected in this order from oxide/gas interface to metal/oxide interface [24,25]. Based on thermodynamic simulation presented here and phase diagrams thermodynamic calculated [22,23] we can assume that in the present alloy, the Mn_2O_3(corundum) is stable at 800 °C from atmospheric pressure up to $p(O_2)$ close to 10^{-6} and MnO (halite) is stable between $10^{-19} < p(O_2) < 10^{-18}$. Mn_3O_4 is a tetragonal spinel, differing from cubic Mn/Cr spinel by the small chromium solubility, in the presence of chromium. Although is impossible distinguish between both spinels at Figure 4, as the cubic spinel is stable in a wide range of $p(O_2)$, the $p(O_2)$ range where Mn_3O_4 tetragonal spinel formation is expected can be estimated as between approximately $10^{-18} < p(O_2) < 10^{-6}$, the range where the other Mn-rich oxides, MnO and Mn_2O_3 are not stable. This can explain the Mn_3O_4 placement (when this oxide is formed) between external Mn_2O_3 and internal $MnCr_2O_4$ spinel, making difficult the characterization.

Regarding the features observed by SEM image (Figure 3) were already reported before for similar Fe-Mn-Si-Cr-Ni alloys (horizontal cracks, roughness at metal/oxide interface, characteristic metallic layer between the oxide and the original substrate, and some defects and a lot of globular oxide particles); the only exception is related to the internal oxidation. The horizontal cracks were reported to be the cause of oxide delamination in an Fe-17Mn-Si-Cr-Ni-VC alloy, generating oxide spallation [13]. In the present case, no mass loss occurred, probably due to the mechanical anchoring [13] from the metal/oxide roughness, which was observed after cyclic and isothermal oxidation for these alloys [5,7,13]. The layer formed

between the oxide scale and the metallic substrate as already mentioned was reported to be a ferrite layer in similar alloys, formed due to the Mn depletion during the alloy oxidation [5,7,11,13], in good agreement with XRD results presented in Figure 2. However, the internal oxidation observed in this layer will be discussed in more details in a next Section as it was reported for the first time in these alloys.

Oxidation at 1000 °C

The oxides observed after oxidation at 1000 °C and determined by XRD and EDS (Figures 5, 7 and 8) differ from those observed at 800 °C by the absence of Mn_2O_3, and the presence of tetragonal spinel and silica. These results are in accordance with thermodynamic simulation (Figure 9), except for the absence of corundum M_2O_3 structure. At Mn-Cr-O diagrams [22,23] no Mn_2O_3 is expected (contrarily from Thermo-Calc simulation at Figure 9). However, the Mn-Cr-O phase diagrams does not consider, obviously, the influences of Fe, Si and others elements present in the alloy. Considering the oxides determined in the thermodynamic simulation studies of Mn-Cr-O phase diagram, already cited [22,23], the only oxide stable at this temperature, considering initial Cr/(Mn+Cr) ratio (around 0.45) is the cubic spinel. This phase admits all chemical compositions between Mn_3O_4 and Cr_3O_4 ($Mn_xCr_{3-x}O_4$, where $0 \leq x \leq 3$), depending on $p(O_2)$. Another oxide stable at 1000 °C in the Mn-Cr-O phase diagrams is the tetragonal spinel (Mn_3O_4) with small Cr solubility. This spinel is expected as Cr/(Mn+Cr) ratio decreases, fact that probably occurs here due to the fast manganese diffusion, explaining XRD results. As discussed before the Mn-Cr spinel composition cannot be easily determined. EDS results show that the Cr and Mn amount vary at each point, suggesting that $Mn_xCr_{3-x}O_4$ (where $0 \leq x \leq 3$) is the best chemical representation of this layer, corroborating the XRD results. Finally, metallic substrate peaks were also observed in this temperature, and despite the thick oxide layer, the defects allowed ferrite indexation.

Comparing the results obtained after oxidation at 1000 °C with those for the oxidation at 800 °C, the first observed difference is the presence of Cr all over the oxide layer, explaining the higher depletion of this element in the ferrite layer. Another difference is related to Si presence at metal/oxide interface (notice the Si EDS map in Figure 8). Considering the higher amount of O in these regions, some silica oxide probably was formed, as suggested by the present thermodynamic simulation (Figure 9) and XRD analysis (Figure 5). This was possible because at 1000 °C the higher presence of Cr in the oxide layer promotes it depletion and, jointly with Mn depletion, increases the content of Si available in the alloy to form the oxide. Furthermore, the high chromium presence probably decreases the $p(O_2)$ at the metal/oxide

interface, important condition to form SiO_2 (tridymite at Figure 9). However, the high roughness at metal/oxide interface, as discussed before, emphasized by cyclic oxidation [16], promoting defects and internal oxidation, probably do not allow the formation of a continuous silica layer, which could act as an additional diffusion barrier, thus decreasing the oxidation rate of the alloy. Furthermore, for conventional austenitic stainless steel it was observed discontinuous silica layer, explained by the higher Si diffusivity in the grain boundaries than in the lattice [26]. Perhaps, in isothermal long-term studies this silica layer formation could be interesting.

Internal oxidation

The internal oxidation observed here in the ferrite layer was more evident and intense after oxidation at 1000 °C, fact explained by the higher O activity and diffusivity. This behaviour was never reported in previous studies for Fe-Mn-Si-Cr-Ni alloys [4–9,13], but in all cases the amount of Mn was higher (12.32 to 17 wt.%) than here (12 wt.%) and/or the oxidation periods were in several studies limited to a maximum of 120 h. The internal oxidation is caused normally by a selective oxidation of an element (as is the present case for Mn), which does not diffuse quickly to the surface while the region beneath the oxide scale becomes depleted in it [27]. The exposure time to oxidizing atmosphere can also influence as mentioned by Douglass *et al*. [28], which not observed internal oxidation for short periods of oxidation in an Fe-Mn-Cr. Although several studies performed shorter oxidation tests (up to 120 hours) [4–6,8,9], as mentioned before, for the Fe-17Mn-Si-Cr-Ni-VC alloy no internal oxidation was observed at longer oxidation periods at 900 °C (987 cycles) [13], or at 800 °C (1218 cycles) [29], as also for an Fe-13.58Mn-Si-Cr-Ni-Ce alloy oxidized more than 250 cycles at 850 °C [7]. These results corroborate the idea that the lower amount of Mn in the present alloy generated this behavior. Regarding to the voids presented in the Mn-depleted layer, selective oxidation can also be the responsible because the diffusion rates of Mn and other elements are different, generating accumulation of vacancies that evolve to voids both inside the grains and the grain boundaries, as observed, for example, in selective oxidation of aluminum in Ni-based alloys [27,30,31].

In a previous study [16], investigating the increase of roughness at the metal/oxide interface in an Fe-Mn-Si-Cr-Ni alloy, it was determined that besides the thermo-mechanical effects proposed before, a chemical effect was also observed, based on reported study of an Fe-Mn-Cr alloy [28] and explained by usual diffusion laws. The roughness at the metal/oxide interface increases because the Mn cation diffusion rate in the oxide layer is higher than Mn

diffusion rate in the alloy, mainly because of the Mn depletion in the ferrite layer. However, this formation of globular oxide protrusions at ferrite layer [16], reported as internal oxidation for an Fe-Mn-Cr alloy [28] and explained also in terms of Mn depletion, was different of the observed here, as it was physically connected to the continuous oxide layer. Here, it seems that the internal oxides are surrounded by metallic substrate. As the alloy studied here presents only 12 wt.% of Mn and its depletion achieves final values around 1.2 wt.%, this internal oxidation could be observed, contrarily from the observed for a higher Mn-containing Fe-17Mn-5Si-10Cr-4Ni alloy, tested at 900 °C up to 987 cycles [13]. In other words, in alloys with higher manganese, due to this chemical diffusion effect, the Mn depletion is enough to create protrusions in the oxide layer which advances in the metal substrate at metal/oxide interface but these protrusions make part of oxide layer. Here, as the manganese content in this alloy is small this chemical diffusion effect leads to internal oxidation as the Mn depletion near the metal/oxide interface achieves critical values.

Besides the aforementioned reasons causing the internal oxidation, as pointed before, the internal oxidation observed in an Fe-Mn-Cr alloys [28] was physically connected with the external oxide layer, justifying the formation of the same oxides. Here, the presence of the same oxides separated from the external oxide layer should be better discussed. Evaluating internal oxidation in deep, it is a phenomenon often related to different values of $p(O_2)$, generating internal oxidation with different oxides (present internally) compared to those present at the continuous and external oxide layer. For example, in Ni-Cr superalloys containing small amount of aluminum, an external Cr_2O_3 layer is often formed, decreasing oxygen activity and promoting Al_2O_3 internal oxidation [27]. On the other hand, here, the internal oxides are the same observed in the external oxide layer. Considering that $MnCr_2O_4$ is stable even for $p(O_2) = 10^{-27}$ (remarkably low) and is the most stable phase at $p(O_2) < 10^{-18}$ (Figure 3), and as Mn-rich oxides Mn_2O_3 and Mn_3O_4 are stable only for $p(O_2)$ around 10^{-18} or higher is not reasonable assume that oxygen pressure in the internal oxides is lower than at external layer.

The mechanism for internal oxidation in this study can be associated with the manganese depletion but is also necessary an easier path for oxygen diffusion, as $MnCr_2O_4$ layer formed at metal/oxide interface is known by avoid internal oxidation in these alloys. Two main aspects can be related to the oxygen diffusion and the first one is related to Cr-depletion. As observed in Ni-Cr alloys [32], the Cr-depletion, demonstrated here in the ferrite layer, can promote voids close to metal/oxide interface and close to grain boundaries, that are the preferential diffusion path for Cr. These voids allow oxygen transport with relatively high partial pressure. The second aspect is concerned to cyclic oxidation, which can promote oxide

layer failures by heating/cooling alternance, generating metal/oxide interface deformation and oxide fracture/spallation, as previously observed in similar alloys [13,15,16], and supported by the cracks observed (Figure 3, 6 and 7) and the anomalous behavior of mass variation observed at 900 °C (Figure 1). Thus, these defects can break the continuous spinel layer and expose the Mn-depleted ferrite layer to a high oxygen partial pressure, promoting oxygen inward and forming Mn-rich oxides inside the substrate. Is interesting to mention that even with internal oxidation, no Fe-rich oxide is observed, showing that Cr/Mn spinel is formed protecting the substrate from catastrophic oxidation.

Based on the considerations regarding internal oxidation, the mass variation curves and the EDS and XRD results, it can be inferred that the smaller amount of Mn and its depletion during the oxidation is not enough to decrease oxidation rate in cyclic oxidation tests. Further isothermal studies in long exposure periods at high temperature should be performed to evaluate if the behavior of internal oxidation (as protrusions or as separated oxide particles) also occurs or if in a condition of low mechanical stresses (promoted by cyclic oxidation), a more protective oxide layer can be formed. SiO_2, predicted as a possible oxide in both temperatures and observed after oxidation at 1000 °C can also improve the oxidation resistance if forms continuously. However, was evidenced here that if the oxide layer does not avoid critical manganese depletion, the internal oxidation occurs due to the low content of manganese in the ferrite layer.

Conclusions

The cyclic oxidation tests at 800, 900 and 1000 °C, showed that Fe-12Mn-5Si-9Cr-4Ni-NbC alloy presented parabolic oxidation behavior in terms of mass gain by surface area, with k_p values similar to alloys with higher Mn content than the current one. Oxide layers were characterized after tests at 800 and 1000 °C, demonstrating higher amount of Mn and Cr. Thermodynamic simulations predicted mainly M_2O_3, M_3O_4 and SiO_2 oxides for both temperatures. At 800 °C the oxides identified were Mn_2O_3 and Mn-Cr spinel, but no SiO_2, while at 1000 °C different Mn-Cr spinels were observed with strong evidence of silica, together with higher amount of Cr in the scale, showing accordance with thermodynamic simulation except by the M_2O_3 absence. The formation of a ferrite layer due to Mn depletion was observed, presenting an almost flat interface with the austenite base material, but a rough interface with the oxide layer. Internal oxidation was also evident in this ferrite layer, phenomenon that not reached the base material. As the oxides formed in the internal oxidation were the same observed at external oxide layer, the mechanism proposed emphasizes defects generated by

thermal cycles that allow high partial pressure in contact to Mn-depleted ferrite layer. These findings demonstrate that decreasing Mn content is not a good solution to increase the oxidation resistance of Fe-Mn-Si-Cr-Ni shape memory stainless steels in cyclic oxidation, since the Mn depletion can increase the metal/oxide interface roughness and promote internal oxidation. However, further studies should be performed at isothermal long-term oxidation tests, as formation of a continuous silica layer in the absence of mechanical stresses could improve the oxidation behavior.

Acknowledgements

AMSM would like to acknowledge the support of the National Council of Technological and Scientific Development – CNPq – Brazil through a PhD scholarship (2009–2013), process number: 140634/2009-6, Materials Institute of Brazil – MIB for the research support and European Comission for Erasmus Mundus scholarship during 10 months during doctorate – EBW2 (2010-2011) at UPC-Spain.JMC thanks CONACyT (Mexico) for partial funding his sabbatical leave in UMSNH. Finally, we would like to acknowledge M.Sc. Bruno Xavier de Freitas and Prof.Dr. Gilberto Carvalho Coelho from USP/EEL - University of São Paulo (USP) – Lorena School of Engineering (EEL) – Department of Materials Engineering (DEMAR) by the thermodynamic calculations.

Data availability

The raw/processed data required to reproduce these findings cannot be shared at this time due to technical or time limitations.

References

[1] K.K. Alaneme, E.A. Okotete, Reconciling viability and cost-effective shape memory alloy options – A review of copper and iron based shape memory metallic systems, Eng. Sci. Technol. an Int. J. 19 (2016) 1582–1592. https://doi.org/http://dx.doi.org/10.1016/j.jestch.2016.05.010.

[2] H. Otsuka, H. Yamada, T. Maruyama, H. Tanahashi, S. Matsuda, M. Murakami, Effects of Alloying Additions on Fe-Mn-Si Shape Memory Alloys, ISIJ Int. 30 (1990) 674–679. https://doi.org/10.2355/isijinternational.30.674.

[3] J.C. Li, X.X. Lü, Q. Jiang, Shape memory effects in an Fe14Mn6Si9Cr5Ni alloy for joining pipe, ISIJ Int. 40 (2000) 1124–1126. https://doi.org/10.2355/isijinternational.40.1124.

[4] R. Silva, C. Arana, A.M. de Sousa Malafaia, A.A. Mendes Filho, C. Pascal, J. Otubo, V.L. Sordi, C.A.D. Rovere, Microstructure and surface oxidation behavior of an austenitic Fe-Mn-Si-Cr-Ni-Co shape memory stainless steel at 800 °C in air, Corros. Sci. 158 (2019)

108103. https://doi.org/10.1016/J.CORSCI.2019.108103.

[5] R. Ma, H. Peng, Y. Wen, L. Zhang, K. Zhao, Oxidation behavior of an austenitic stainless FeMnSiCrNi shape memory alloy, Corros. Sci. 66 (2013) 269–277. https://doi.org/http://dx.doi.org/10.1016/j.corsci.2012.09.029.

[6] R. Silva, G.S. Vacchi, I.G.R. Santos, A.M. de Sousa Malafaia, C.L. Kugelmeier, A.A. Mendes Filho, C. Pascal, V.L. Sordi, C.A.D. Rovere, Insights into high-temperature oxidation of Fe-Mn-Si-Cr-Ni shape memory stainless steels and its relationship to alloy chemical composition, Corros. Sci. 163 (2020) 108269. https://doi.org/10.1016/j.corsci.2019.108269.

[7] V.F. de Souza, A.J. Araújo, J.L. do N. Santos, C.A. Della Rovere, A.M. de S. Malafaia, Kinetics Oxidation and Characterization of Cyclically Oxidized Layers at High Temperatures for FeMnSiCrNiCe and FeSiCrNi Alloys, Mater. Res. 20(Suppl. (2017) 365–373. https://doi.org/10.1590/1980-5373-mr-2017-0098.

[8] A.M. de Sousa Malafaia, L. Latu-Romain, Y. Wouters, High temperature oxidation resistance improvement in an FeMnSiCrNi alloy by Mn-depletion under vacuum annealing, Mater. Lett. 241 (2019) 164–167. https://doi.org/10.1016/j.matlet.2019.01.074.

[9] Y. Jiao, H. Zhang, Y. Wen, Influence of Temperature on the Oxidation Behaviour of an Austenitic Stainless FeMnSiCrNi Shape Memory Alloy, Oxid. Met. 92 (2019) 109–121. https://doi.org/10.1007/s11085-019-09916-y.

[10] B. Qian, H. Peng, Y. Wen, A novel sandwich Fe-Mn damping alloy with ferrite shell prepared by vacuum annealing, Smart Mater. Struct. 27 (2018) 45005. https://doi.org/10.1088/1361-665X/aaaf95.

[11] G. Coccia Lecis, C. Lenardi, A. Sabatini, The effect of Mn-depleted surface layer on the corrosion resistance of shape memory Fe-Mn-Si-Cr alloys, Metall. Mater. Trans. A. 28 (1997) 1219–1222. https://doi.org/10.1007/s11661-997-0287-z.

[12] H. Peng, J. Hua, B. Xu, Y. Wen, Fabrication of Ferrite-Coated Magnetic Fe–Mn–Si–Cr–Ni Alloy Utilizing Selective Oxidation of Mn Element, IEEE Trans. Magn. 55 (2019) 1–7. https://doi.org/10.1109/TMAG.2019.2904568.

[13] A.M. de Sousa Malafaia, M.F. de Oliveira, Anomalous cyclic oxidation behaviour of a Fe–Mn–Si–Cr–Ni shape memory alloy, Corros. Sci. 119 (2017) 112–117. https://doi.org/10.1016/j.corsci.2017.02.026.

[14] S. Baleix, G. Bernhart, P. Lours, Oxidation and oxide spallation of heat resistant cast steels for superplastic forming dies, Mater. Sci. Eng. A. 327 (2002) 155–166. https://doi.org/http://dx.doi.org/10.1016/S0921-5093(01)01529-5.

[15] A.M. De Sousa Malafaia, V.R. do Nascimento, L. Mendes Sousa, M. E. Silveira, M.F. de Oliveira, Anomalous cyclic oxidation behaviour of an Fe-Mn-Si-Cr-Ni alloy - A finite element analysis, Corros. Sci. 147 (2019) 223–230. https://doi.org/10.1016/j.corsci.2018.11.018.

[16] L.F.P. Rabelo, R. Silva, C.A. Della Rovere, A.M. de Sousa Malafaia, Metal/oxide interface roughness evolution mechanism of an FeMnSiCrNiCe shape memory stainless steel under high temperature oxidation, Corros. Sci. 163 (2020). https://doi.org/10.1016/j.corsci.2019.108228.

[17] J. Wadsworth, S.R. Keown, J.H. Woodhead, The effect of niobium carbide precipitation on the density changes and creep properties of Type 347 austenitic stainless steels, Met. Sci. 10 (1976) 105–112. https://doi.org/10.1179/msc.1976.10.3.105.

[18] M. Taneike, F. Abe, K. Sawada, Creep-strengthening of steel at high temperatures using nano-sized carbonitride dispersions, Nature. 424 (2003) 294–296. https://doi.org/10.1038/nature01740.

[19] S.H. Wang, Y.H. Wen, W. Zhang, N. Li, Improvement of shape memory effect in an Fe–Mn–Si–Cr–Ni–Nb–C alloy by NbC precipitated through ageing after pre-deformation, J. Alloys Compd. 437 (2007) 208–210. https://doi.org/10.1016/J.JALLCOM.2006.07.060.

[20] A.M.S. Malafaia, M.T. Milan, M. Omar, R.M. Muñoz Riofano, M.F. De Oliveira, Oxidation and abrasive wear of Fe-Si and Fe-Al intermetallic alloys, J. Mater. Sci. 45 (2010). https://doi.org/10.1007/s10853-010-4591-4.

[21] J.R. Nicholls, M.J. Bennett, Cyclic oxidationguidelines for test standardisation, aimed at the assessment of service behaviour, Mater. High Temp. 17 (2000) 413–428. https://doi.org/10.3184/096034000783640758.

[22] I. Jung, Critical evaluation and thermodynamic modeling of the Mn – Cr – O system for the oxidation of SOFC interconnect, Solid State Ionics. 177 (2006) 765–777. https://doi.org/10.1016/j.ssi.2006.01.012.

[23] L. Kjellqvist, M. Selleby, Thermodynamic assessment of the Cr – Mn – O system, J. Alloys Compd. 507 (2010) 84–92. https://doi.org/10.1016/j.jallcom.2010.04.252.

[24] J. Païdassi, A. Echeverría, Sur l'oxydation du manganese dans l'air aux température élevées, Acta Metall. 7 (1959) 293–295. https://doi.org/10.1016/0001-6160(59)90024-0.

[25] H. Buscail, J.P. Larpin, The Influence of Ceria Surface Additions on Manganese Oxidation at High Temperatures, Oxid. Met. 43 (1995) 237–261.

[26] A. Col, V. Parry, C. Pascal, Oxidation of a Fe–18Cr–8Ni austenitic stainless steel at 850 °C in O2: Microstructure evolution during breakaway oxidation, Corros. Sci. 114 (2017) 17–27. https://doi.org/10.1016/J.CORSCI.2016.10.029.

[27] D.J. Young, High Temperature Oxidation and Corrosion of Metals, Elsevier, 2016. https://doi.org/10.1016/C2014-0-00259-6.

[28] D.L. Douglass, F. Gesmundo, C. de Asmundis, The air oxidation of an austenitic Fe-Mn-Cr stainless steel for fusion-reactor applications, Oxid. Met. 25 (1986) 235–268. https://doi.org/10.1007/BF00655899.

[29] A.M. de S. Malafaia, Oxidação cíclica em alta temperatura de ligas ferrosas fundidas de baixo custo - PhD thesis [in Portuguese], 2013. https://doi.org/10.11606/t.18.2013.tde-15012014-103642.

[30] R.P. Oleksak, M. Kapoor, D.E. Perea, G.R. Holcomb, Ö.N. Doğan, The role of metal vacancies during high-temperature oxidation of alloys, Npj Mater. Degrad. 2 (2018) 1–8. https://doi.org/10.1038/s41529-018-0046-1.

[31] F.H. Stott, G.C. Wood, Y. Shida, D.P. Whittle, B.D. Bastow, The development of internal and intergranular oxides in nickel-chromium-aluminium alloys at high temperature,

Corros. Sci. 21 (1981) 599–624. https://doi.org/10.1016/0010-938X(81)90011-1.

[32] Y. Shida, G.C. Wood, F.H. Stott, D.P. Whittle, B.D. Bastow, Intergranular oxidation and internal void formation in Ni-40% Cr alloys, Corros. Sci. 21 (1981) 581–597. https://doi.org/10.1016/0010-938X(81)90010-X.

Figure Captions

Figure 1 – a) mass variation during cyclic oxidation tests at 800, 900 and 1000 °C and in detail (a') the parabolic fitting during the initial cycles; b) square root transform to determination of parabolic constants k_p values for all temperatures and in detail (b') the Arrhenius plot for the activation energy determination.

Figure 2 – XRD analysis performed on top surface of Fe-12Mn-5Si-9Cr-4Ni-NbC oxidized at 800 °C after 749 cycles.

Figure 3 – Cross-section SEM/EDS analyses of Fe-12Mn-5Si-9Cr-4Ni-NbC alloy oxidized at 800 °C,during 749 cycles, detailing oxide layer with horizontal cracks, a ferrite layer, internal oxidation and oxygen, manganese, chromium, silicon and iron element maps.

Figure 4 – Mole fraction expected for each phase in equilibrium (wt.%) at 800 °C *versus* $p(O_2)$; thermodynamic simulation performed using Thermo-Calc with the TCFE7 database.

Figure 5 – XRD diffractogram performed on top surface of sample oxidized at 1000 °C during 383 cycles.

Figure 6 – SEM cross-section images of the sample oxidized during 383 cycles at 1000 °C, showing an overview (a) and more detailed high magnification (b).

Figure 7 – Detailed SEM/EDS analysis of sample oxidized at 1000 °C during 383 cycles: (a) SEM image with EDS points, followed by EDS elemental maps: oxygen, manganese, silicon, chromium and iron.

Figure 8 – SEM/EDS analysis at metal/oxide interface region, after oxidation at 1000 °C, detailing silicon oxide formation.

Figure 9– Mole fraction expected for each phase in equilibrium (wt.%) at 1000 °C *versus* $p(O_2)$; thermodynamic simulation performed using Thermo-Calc with the TCFE7 database.

Figure 10 – Neperian logarithms of k_ps by the inverse of temperature (Arrhenius plot) comparing present article data (diamonds) with literature data from [4–9,13]; open and filled symbols represent cyclic and isothermal tests, respectively.